Enhancing the Storage Performance and Thermal Stability of Ni-rich Layered Cathodes by Introducing Li_2MnO_3

Jun Yang *, Pingping Yang , Hongyu Wang

Posted Date: 5 January 2024

doi: 10.20944/preprints202401.0450.v1

Keywords: lithium-ion batteries; Ni-rich cathode; storage performance; thermal stability; Li2MnO3

Article

Enhancing the Storage Performance and Thermal Stability of Ni-rich Layered Cathodes by Introducing Li_2MnO_3

Jun Yang [1,*], Pingping Yang [1] and Hongyu Wang [2]

[1] School of Materials Science & Engineering, Shaanxi Key Laboratory of Green Preparation and Functionalization for Inorganic Materials, Shaanxi University of Science & Technology, Xi'an, Shaanxi 710021, People's Republic of China

[2] Qinghai Provincial Key Laboratory of New Light Alloys, Qinghai University, Xining, Qinghai, 810016, People's Republic of China

* Correspondence: yangjuncl@sust.edu.cn

Abstract: Ni-rich layered cathodes are regarded as a potential candidate for high energy-density lithium-ion batteries, but their high sensitivity to air during storage and poor thermal stability are a vital challenge for large-scale applications. In this paper, an effective solid-solution strategy was proposed to improve the surface and structural stability of Ni-rich layered cathodes by introducing Li_2MnO_3. The structural analysis results indicate that the formation of Li_2CO_3 inert layers on Ni-rich layered cathodes during storage in air is responsible for the increased electrode interfacial impedance, thereby resulting in the severe deterioration of electrochemical performance. The introduction of Li_2MnO_3 can reduce the surface reactivity of Ni-rich cathode materials, playing a certain suppression effect on the formation of surface Li_2CO_3 layer and the deterioration of electrochemical performances. Additionally, the thermal analysis results show that the heat release of Ni-rich cathodes strongly depends on the charge of states, and Li_2MnO_3 can suppress oxygen release and significantly improves the thermal stability of Ni-rich layered cathodes. This work provide a method to improve the storage performance and thermal stability of Ni-rich cathode materials.

Keywords: lithium-ion batteries; Ni-rich cathode; storage performance; thermal stability; Li_2MnO_3

1. Introduction

As a renewable and efficient energy storage system, lithium-ion batteries (LIBs) have been widely applied in the fields of portable electronic products, intelligent power stations, and electric vehicles (EVs). In particular, the commercialization of EVs requires the development of advanced LIBs technology. In this regard, Ni-rich layered oxides are considered promising cathode materials for LIBs due to their high reversible capacity (200 mA h g^{-1}) [1,2]. However, a critical challenge of Ni-rich cathodes is the surface instability induced by high chemical reactivity [3]. When exposed to air, Ni-rich cathode materials tend to react chemically with CO_2 and H_2O in the atmosphere, forming Li_2CO_3/LiOH impurities on secondary particles. This surface contamination of Ni-rich cathode materials exhibits a low ionic conductivity for Li^+ transportation. Thus, the interfacial charge transfer resistance is increased and a loss of reversible capacity is induced [4–6]. More seriously, the surface Li-derives impurities accelerate the harmful side reactions between electrolyte and the active surface of cathodes. The electrochemical oxidation of Li_2CO_3 produces intermediate free radicals which react rapidly with the electrolyte solvent, triggers the decomposition of the electrolyte, releasing gaseous products and producing solid-state products on the cathode surface. Meanwhile, the acidic products produced by the chemical decomposition of electrolytes attack cathode surface results in the dissolution of transition metal ions (TMs) [7–9]. These harmful chemical behaviors induced by surface Li-derived impurities exacerbate the deterioration of electrochemical properties [10–12]. In addition, the thermal instability of the Ni-rich cathode also poses a safety risk for LIBs in practice [13]. In a highly delithiated Ni-rich cathode, metastable Ni^{4+} ions weaken the Ni-O bonds and thereby

increase the reactivity of lattice oxygen, as their covalence increases. Driven by elevated temperature and high delithiated states, the lattice oxygen release is aggravated to induce the reduction of Ni^{4+} to Ni^{2+} ions, accompanied by the structural degradation from layered to spinel phase and finally to rock-salt phase [14,15]. Subsequently, reacting with flammable electrolytes, the highly reactive oxygen species released from the Ni-rich cathode accelerate the combustion of electrolytes to cause thermal runaway and release a large number of harmful gaseous products. Therefore, it is concluded that the unsatisfactory storage performance and thermal stability of the Ni-rich cathode are strongly linked with the structure instability resulting from the high Ni-content and active Ni-O bonds in the layered cathode.

As a common modification strategy to improve structure stability, surface coating can effectively isolate the active cathode surface from the electrolyte, preventing the serious interfacial side reactions [16–19]. Moreover, it has been demonstrated coating can eliminate surface residual Li-derived impurities and inhibit the immigration of active lattice Li^+ into the surface during storage in air, displaying an improved effect on storage performance. However, surface coating has less influence on the reactivity of lattice oxygen in the bulk due to no change in composition and crystal structure, thereby implying a limited improvement in the thermal stability of cathode materials. Additionally, a critical concern also needs to be considered that the poor interfacial compatibility between coating materials and layered cathode hinders Li^+ ions' fast transport. Composition optimization is regarded as an effective strategy for improving the structural and thermal stability of cathode materials, which is extensively investigated by Sun's group [20]. Mn element has been proven to be a remarkable enhancement of the thermodynamics stability of layered cathodes. Hence, increasing Mn content and decreasing Ni content in surface composition can significantly reduce the surface chemical reactivity of the Ni-rich cathode, achieving excellent structure stability. In our previous research, introducing a low-content layered L_2MnO_3 into Ni-rich layered cathode to form the layered solid-solution, exhibits prominently improved structural stability of layered cathode at high-voltage by suppressing the phase transition [21,22]. As a structural stabilizer, Li_2MnO_3 not only significantly reduces variations of unit-cell volume to stabilize the original layered structure of Ni-rich cathode, but also passivates the active surface by increasing Mn content and decreasing Ni content on the cathode surface. Despite this, it has still less investigation on evaluating the storage performance and thermal stability of these solid solution cathode materials.

Based above considerations, a low-content Li_2MnO_3 was introduced into the Ni-rich cathode to form a solid-solution cathode, reducing their surface reactivity. The influence of introducing Li_2MnO_3 on storage performance and thermal stability of Ni-rich cathode were further investigated in this work. The variations in surface/interface structure and electrochemical performance of Ni-rich cathode during storage in air were explored in detail to build the strong structure-properties correlations. Comparatively, the Ni-rich cathode modified with Li_2MnO_3 exhibits a suppressed formation of surface Li_2CO_3 inert layers and low interfacial electrode resistance, which accounts for their inhibitory effect on the deterioration of electrochemical performance. Furthermore, the delithiation potentials and introduction of Li_2MnO_3 on the thermal stability of Ni-rich layered cathode were investigated by differential scanning calorimeter (DSC). The solid-solution cathode presents a relatively low heat release related to weak phase transition. This work contributes a insightful understanding of the storage performance and thermal stability of solid-solution cathode.

2. Materials and Methods

2.1. Samples Synthesis

Ni-rich layered cathode materials were prepared via a co-precipitation followed by sintering at high temperatures. Firstly, the hydroxide precursors $(Ni_{0.8}Co_{0.1}Mn_{0.1})(OH)_2$ were synthesized via a co-precipitation method [21–23]. Three sulfates ($NiSO_4{\cdot}6H_2O$, $CoSO_4{\cdot}7H_2O$, and $MnSO_4{\cdot}H_2O$) were dissolved in distilled water at the molar ratio of 8/1/1 (Ni/Co/Mn) to form a mixed solution with a concentration of 1 M. Then, a reaction base solution (pH = 11~12) was heated at 55 °C under N_2 protection. Then, the mixed metal ions solution (1M) and NaOH solution (2M) were synchronously

added to the base solution for co-precipitation reaction. After the reaction was complete, the products was collected and then washed with distilled water. Finally, the hydroxide precursor $(Ni_{0.8}Co_{0.1}Mn_{0.1})(OH)_2$ was obtained after drying at 120 °C for 12 h. Similarly, the precursor $(Ni_{0.8}Co_{0.1}Mn_{0.1})_{0.9}Mn_{0.1}(OH)_2$ was also prepared by regulating the ratio of three sulfates via the same synthesis process. Then, the precursor powder and $LiOH{\cdot}H_2O$ were mixed and sintered at 480 °C for 5 h and 750 °C for 15 h under O_2 atmosphere, respectively. Finally, the as-obtained $LiNi_{0.8}Co_{0.1}Mn_{0.1}O_2$ and solid-solution cathode $0.1Li_2MnO_3{\cdot}0.9LiNi_{0.8}Co_{0.1}Mn_{0.1}O_2$ were denoted as NCM-811-Fresh and LNCMO-1090-Fresh, respectively. Furthermore, the as-synthesized cathode materials were exposed to air for 6 months and denoted as NCM-811-Air and LNCMO-1090-Air.

2.2. Materials Characterization

Powder X-ray diffraction (XRD) measurements were performed to identify the crystal structure of the cathode materials by X-ray diffractometer using a Cu-Kα radiation source (Bruker, Germany), and carried out in the 2θ range of 10° ~ 100°. The surface chemical environment of cathode materials was characterized by X-ray photoelectron spectroscopy (XPS), which was performed on the PHI5000C system with a Kα source operating at 14.0 kV and 25 mA. The energy of the XPS spectrum is calibrated with the binding energy of C 1s at 284.6 eV. The surface morphology of the samples was observed by scanning electron microscope (SEM, JEOL JEM-6390) at a voltage of 25 kV. High-resolution transmission electron microscopy (HRTEM, JEOL JEM-2100) was used to observe the microstructure of the cathode materials.

2.3. Electrochemical Measurements

Electrochemical measurements were carried out in CR2016-type coin cells. The preparation of electrodes is carried out by the following process. Using carbon black as conductive material and polyvinylidene difluoride (PVDF) as binder, the cathode material was homogeneously mixed in N-methyl-2-pyrrolidone (NMP) solvent with a weight ratio of 8:1:1. Then, the slurry was homogeneously cast on the aluminum foil as current collector. The electrodes were then vacuum-dried at 80 °C for 10 h to remove the solvent. The electrode film was cut into a disks with a diameter of 12 mm. In a glove box filled with pure argon, the half cells were assembled with the prepared cathode, lithium metal as the anode, and Celgard 2300 film as the separator. The electrolyte solution was 1 M $LiPF_6$ dissolved in ethylene carbonate (EC)-dimethyl carbonate (DMC)-ethyl methyl carbonate (EMC) at a volume ratio of 1:1:1. The LAND CT2001A Battery Cycler (Wuhan, China) was used for constant current charging-discharging experiments (1 C = 200 mA g^{-1}) between 2.0 and 4.5 V vs Li/Li^+ at room temperature (25 °C). Electrochemical impedance spectroscopy (EIS) measurements were performed on the Solartron 1287 & Solartron 1255B frequency response analyzer systems in the frequency range of 1 MHz to 1 mHz with amplitude of 5 mV at room temperature.

2.4. Thermal Stability Test

The thermal stability of the cathode material was measured by differential scanning calorimeter (DSC). DSC measurements of electrode materials were performed as following. The assembled cells were charged to the specified voltage and kept at constant voltage for several hours to reach the equilibrium state, and then disassembled in the glove box under argon. The delithiated cathode was removed from the cells, washed several times with DMC, and dried in a glove box under argon at room temperature. Scraped electrode material from current collector and weighed, placed with electrolytes in a stainless steel crucible, and sealed. The crucible with the sample was heated in the differential scanning calorimeter with N_2 as the purge and protective gas. The heating conditions were: 25 °C ~ 350 °C, 5 °C min^{-1}.

Preprints (www.preprints.org) | NOT PEER-REVIEWED | Posted: 5 January 2024 doi:10.20944/preprints202401.0450.v1

3. Results and Discussion

3.1. Structure Change of Ni-rich Cathode During Storage in Air

Benefited from the similar crystal structure between layered Li_2MnO_3 and layered Ni-rich oxide, low-content Li_2MnO_3 is easily incorporated into Ni-rich cathodes to form solid-solution cathodes (LNCMO-1090) by co-precipitation followed by sintering at elevated temperature, which has been confirmed by structure analysis in our previous researches [21,22]. Experimentally, Ni-rich layered cathode materials (NCM-811 and LNCMO-1090) were stored in the air for 6 months. X-ray powder diffraction (XRD) was used to investigate the change in the crystal structure of cathode materials before and after storage, as shown in Figure 1. All observed sharp diffraction peaks of NCM-811-Fresh and NCM-811-Air (Figure 1a) can be indexed based on a layered structure of hexagonal α-$NaFeO_2$ with a trigonal (R-3m) space group symmetry [24], and no other obvious diffraction peaks appear in these cathode materials. Furthermore, some weak diffraction peaks were observed in the XRD spectrum of NCM-811-Air after zooming in the diffraction angle range of 20° ~ 36° (Figure 1c), which was assigned to Li_2CO_3 crystals [25]. When exposed to air, Ni-rich cathode materials tend to react chemically with H_2O/CO_2 in the air due to their high surface reactivity, resulting in the formation of $LiOH/Li_2CO_3$ surface impurities. However, no crystalline LiOH was found in XRD results, which may result from the complete transformation to L_2CO_3 by chemically reacting with CO_2 in air during long-term storage. Furthermore, XRD spectra of LNCMO-1090 before and after storage (Figure 1b) exhibit a set of strong diffraction peaks, which is highly identical to that of NCM-811. This result implies that the layered NCM-811 R-3m phase and the layered Li_2MnO_3 C2/m phase are highly miscible to form a solid solution due to their similar lattice parameter and crystal structure. After magnifying the diffraction range of 2θ = 20° ~ 36° (Figure 1d), some diffraction peaks of Li_2CO_3 crystalline also appear in the XRD pattern of the stored LNCMO-1090-Air. XRD results show Li_2CO_3 impurities are inevitably generated on the Ni-rich cathode surface during storage in the air due to the high sensitivity to air. Given that the XRD technique has low sensitivity to surface structural information, the detailed structure information on the cathode surface after storage needs further be explored further to confirm the thickness of Li_2CO_3 layers on cathode materials.

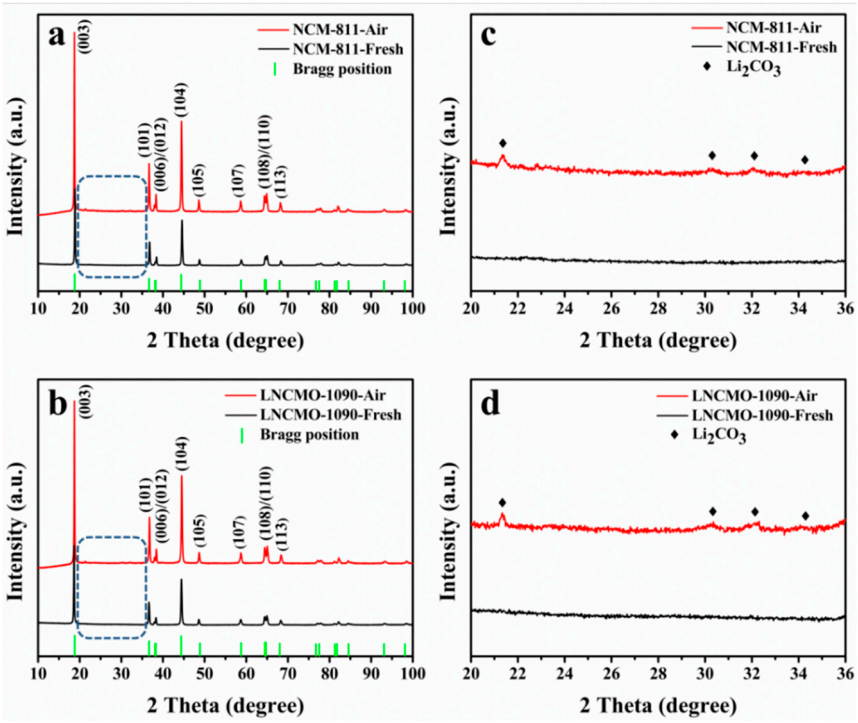

Figure 1. XRD patterns and partial magnifications of cathodes before and after storage: (**a**, **c**) NCM-811; (**b**, **d**) LNCMO-1090.

Preprints (www.preprints.org) | NOT PEER-REVIEWED | Posted: 5 January 2024 doi:10.20944/preprints202401.0450.v1

X-ray photoelectron spectroscopy (XPS) is commonly applied to investigate the surface chemical environment and valence states due to its high sensitivity to the surface structure of materials [26–28]. Hence, the surface structural information of Ni-rich cathode materials was further examined by XPS. Figure 2a and 2b show the C 1s XPS spectra of NCM-811 and LNCMO-1090 before and after storage, and all samples exhibit two peaks in the C 1s spectrum. The peak with a binding energy of 284.6 eV is attributed to contamination of the material surface with a carbon source, which inevitably occurs in all samples. Another peak with a binding energy of 289.7 eV is attributed to a carbon source in the carbonates [3]. For the fresh cathode materials, a very weak CO_3^{2-} peak appears in the C 1s spectra of NCM-811-Fresh and LNCMO-1090-Fresh, which is closely related to the short-time exposure of cathode materials to air after synthesis. This result verifies that Ni-rich layered cathodes have a high surface reactivity and are extremely sensitive to air. After storage in air, NCM-811-Air and LNCMO-1090-Air display a strong peak at 289.7 eV, indicating that a large amount of Li_2CO_3 impurities was generated on the surface of Ni-rich cathode material during storage. Comparatively, the intensity and area of this peak in LNCMO-1090-Air are inferior to that in NCM-811-Air, demonstrating the lower content of Li_2CO_3 impurities on the LNCMO-1090-Air cathode surface. The suppressed effects on Li_2CO_3 impurities formation on the solid-solution cathode (LNCMO-1090) can be attributed to their reduced surface chemical reactivity.

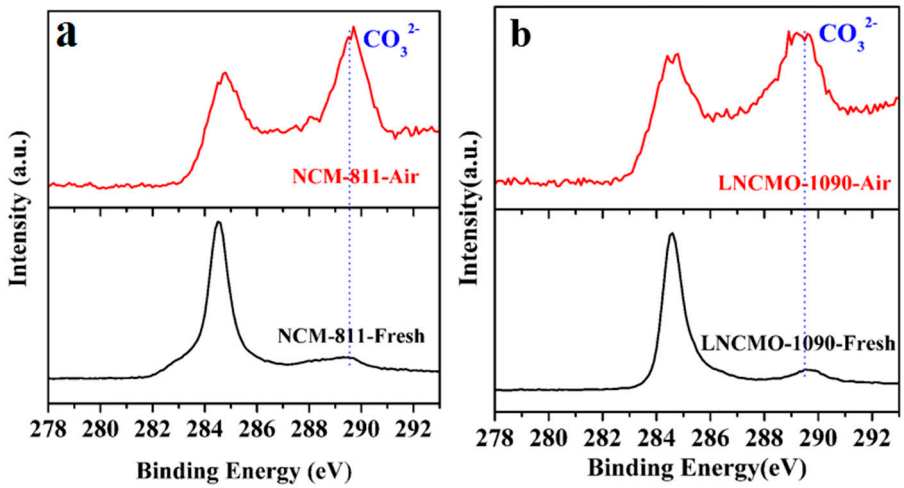

Figure 2. The C 1s XPS spectra of cathodes before and after storage: (**a**) NCM-811; (**b**) LNCMO-1090.

Scanning electron microscopy (SEM) was used to observe the change in surface morphology of Ni-rich layered cathode materials during storage. Figure 3 shows SEM images of NCM-811 and LNCMO-1090 materials before and after storage. Before storage, both NCM-811-Fresh (Figure 3a) and LNCMO-1090-Fresh (Figure 3c) exhibit micron-scale spheroid secondary particles, which are formed by aggregation of primary particles of 200-500 nm. After storage for 6 months in the air, as shown in Figure 3b and Figure 3d, the size and morphology of NCM-811-Air and LNCMO-1090-Air materials have not changed significantly, and they exhibit still micron-scale spheroid aggregates. Therefore, the storage process has less influence on the surface morphology of Ni-rich layered cathode materials, and the detailed surface microstructure of the cathode materials needs to be further characterized by electron microscopy (TEM).

Preprints (www.preprints.org) | NOT PEER-REVIEWED | Posted: 5 January 2024 doi:10.20944/preprints202401.0450.v1

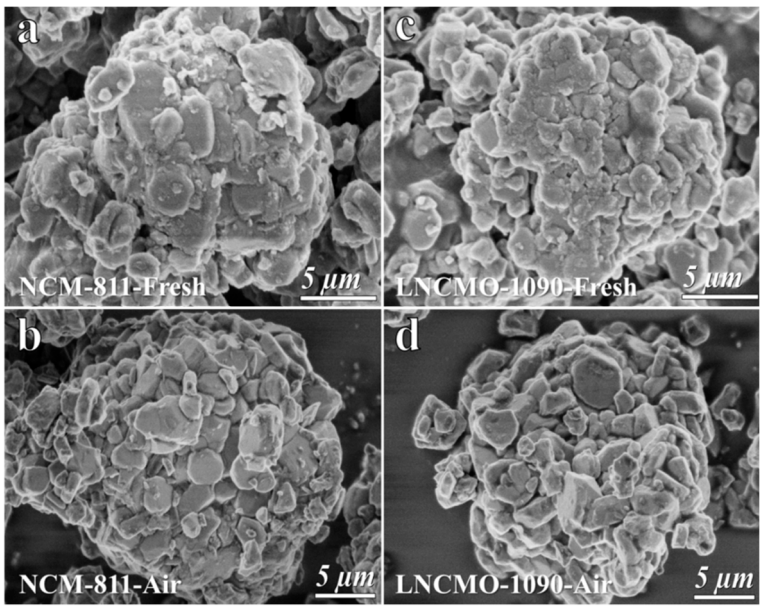

Figure 3. SEM images of cathodes before and after storage: (**a**, **b**) NCM-811; (**c**, **d**) LNCMO-1090.

Figure 4 indicates TEM images of NCM-811 and LNCMO-1090 before and after storage. Before storage, NCM-811-Fresh (Figure 4a) exhibits a layered crystal structure, but its surface structure has changed to produce a clear interfacial structure. In the insets of Figure 4a, the bulk region shows a well-defined layered structure with a lattice distance of 0.48 nm assigned to the (003) crystal facets of the rhombohedral phase, while the surface region displays the lattice fringes with 0.24 nm that respond to (111) crystal facts of cubic rock-salt phase. As a typical characteristic of structural degradation of Ni-rich cathodes, the formation of surface rock-salt phase induced by Ni^{2+} ions migrating into Li^{+} sites generally occurs during synthesis preparation or exposure to air due to the high surface reactivity [29–31]. In contrast, the LNCMO-1090 cathode (Figure 4b) presents a highly ordered layered structure, and consistent lattice fringes with 0.48 nm from surface to bulk region, which is closely correlated to the relatively stable surface of LNCMO-1090. The presence of the Li_2MnO_3 phase increases the Mn-rich region content on the LNCMO-1090 surface, thus improving the surface structural stability of Ni-rich cathodes. Furthermore, it is observed in Figure 4c that thick and dense Li_2CO_3 layers with a thickness of about 5 nm cover on NCM-811-Air cathode surface after storage. These Li_2CO_3 layers also appear on the LNCMO-1090 cathode surface, but their thickness is remarkably reduced (2~3 nm) in Figure 4d. The results indicate that the formation of Li_2CO_3 impurities was suppressed on the LNCMO-1090 cathode surface, which contributed to the reduced surface reactivity due to its surface increased Mn-rich region.

Preprints (www.preprints.org) | NOT PEER-REVIEWED | Posted: 5 January 2024 doi:10.20944/preprints202401.0450.v1

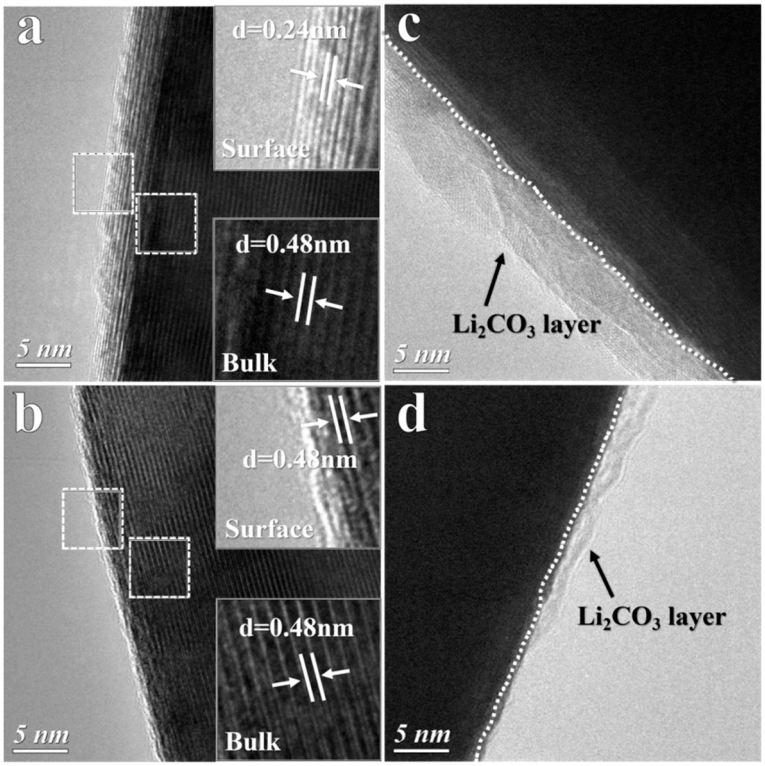

Figure 4. TEM images of cathodes before and after storage: (**a**, **c**) NCM-811; (**b**, **d**) LNCMO-1090.

3.2. Changes in Electrochemical Properties of Ni-rich Cathodes During Storage

To further clarify the change of interfacial structure, we characterized the Ni-rich layered cathode material before and after storage using electrochemical impedance spectroscopy (EIS). As shown in Figure 5, the obtained impedance spectrum consists of two semicircles in the high-frequency and medium-frequency region and an oblique line in the low-frequency region. The semicircle in the high-frequency region is related to the impedance generated by Li^+ passing through the surface film of electrodes (R_f). Whereas the second semicircle in the medium-frequency region is the impedance caused by the interface charge transfer, while the low frequency area oblique line is related to lithium ions diffusion behavior in the material phase [32,33]. The equivalent circuit diagram in Figure 5 is used to analyze and fit the impedance spectrum, and the corresponding fitting results are listed in Table S1. The results indicate that LNCMO-1090-Fresh has a slightly larger R_{ct} value compared to NCM-811-Fresh, which is related to the increased inactive Mn component on the surface [34]. Notably, the electrode impedances of NCM-811-Air and LNCMO-1090-Air after storage have an obvious increase in R_f and R_{ct} values compared to that of NCM-811-Fresh and LNCMO-1090-Fresh before storage. Surface Li_2CO_3 impurities layers on Ni-rich cathodes accelerate the harmful side reactions between electrolyte and the active surface of cathodes to produce the cathode-electrolyte interphase (CEI) layer, thereby hindering Li^+ diffusion to generate a R_f [35–37]. Meanwhile, the interfacial side reaction induces the surface degradation from the layered structure to the rock-salt phase to greatly impede the charge transfer process. As shown in Table S1, the increases in both R_f and R_{ct} value for LNCMO-1090 during storage are remarkably lower than that for NCM-811, indicating the suppressed interfacial side reaction resulting from the thinner Li_2CO_3 impurities layers on LNCMO-1090 surface. The electrode impedance of cathodes after storage increases due to the significant change in their surface/interfacial structure, which immensely affects the electrochemical performance of cathode materials.

Preprints (www.preprints.org) | NOT PEER-REVIEWED | Posted: 5 January 2024 doi:10.20944/preprints202401.0450.v1

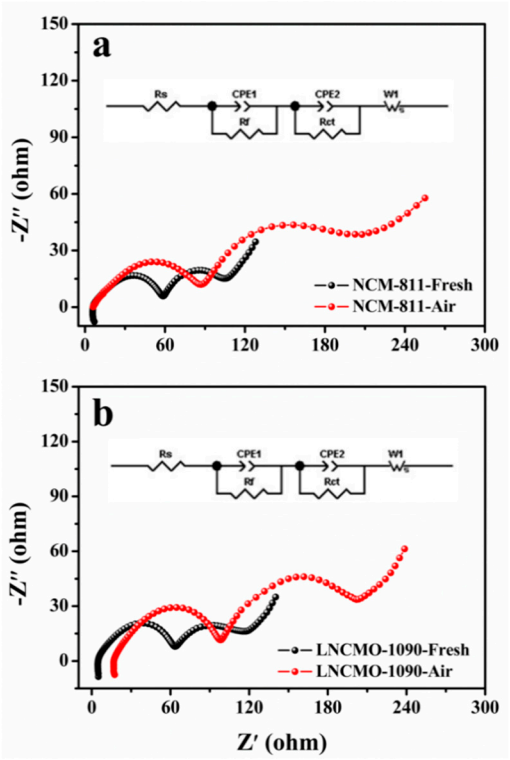

Figure 5. The Nyquist plots and the corresponding equivalent circuit model (inset) of the cathodes charged to 4.3 V before and after storage: (**a**) NCM-811; (**b**) LNCMO-1090.

Furthermore, the variation in the electrochemical performance of cathode materials during storage has been investigated. Figures 6a and 6b show the first charge/discharge curves of NCM-811 and LNCMO-1090 cathode materials before and after storage. An obvious change in discharge/discharge curves was observed in the cathode materials after storage, and the specific capacity at the intersection between charging and discharging curves decreased, indicating that severe polarization behavior occurs in the cathode materials after storage [7,38]. Compared with NCM-811 (Figure 6a), LNCMO-1090 (Figure 6b) has a smaller change in decreasing capacity at the intersection of charge/discharge curves, meaning a slightly weak polarization in the LNCMO-1090-Air. Additionally, the onset potential of the first delithiation of NCM-811 significantly increases after storage (Figure 6a), but it has no obvious change in the LCNMO-1090 cathode (Figure 6b). These observations are closely correlated with the lower electrode impedance of LNCMO-1090-Air, which is ascribed to the thinner surface Li_2CO_3 layer on cathode materials after storage. Consequently, a slight decrease in both charge capacity and discharge capacity was observed in the NCM-811-Air and LNCMO-1090-Air after storage. NCM-811-Fresh and LNCMO-1090-Fresh materials deliver the reversible capacities of 224 mAh g^{-1} and 207 mAh g^{-1}, but their capacities after storage decrease to 219 mAh g^{-1} and 201 mAh g^{-1}, respectively. Furthermore, the cycling performance of the cathode materials before and after storage was evaluated at 0.1C between 2.0 and 4.5 vs Li/Li^+. As shown in Figures 6c and 6d, the NCM-811-Fresh and LNCMO-1090-Fresh before storage show excellent cycling stability with a capacity retention of 82.2% and 84.6% after 50 cycles (Table S2). The excellent cycling stability of fresh cathode materials was also confirmed by the small variation in the charge/discharge profiles during cycling (Figure S1a and S1c). However, the surface Li_2CO_3 impurities on the cathode materials chemically react with electrolyte, leading to continually thickening CEI layers and serious degradation of the surface structure of the electrode. As a result, the cathode materials after storage exhibit deteriorated cycling performance, and the reversible capacities rapidly decrease to 117 mAh g^{-1} for NCM-811-Air and 126 mAh g^{-1} for LNCMO-1090-Air after 50 cycles, which amounts to 53.4% and 62.9 % of initial capacities. Despite the decay in capacities aggravated by surface Li_2CO_3 impurities reacting with electrolyte, LNCMO-1090 exhibits a relatively slow deterioration of cycling performance to NCM-811, which is demonstrated in the change in the charge/discharge curves

Preprints (www.preprints.org) | NOT PEER-REVIEWED | Posted: 5 January 2024 doi:10.20944/preprints202401.0450.v1

during cycling (Figure S1b and S1d). Additionally, the rate capability of cathode materials before and after storage is estimated and shown in Figures 6e and 6f. Upon increasing the rate from 0.1C to 2C, the reversible capacities of NCM-811-Fresh and NCM-811-Air decrease to 138 mAh g^{-1} and 94.5 mAh g^{-1} (Figure S2a and S2b), respectively, which accounts for 62% and 43% of their initial capacities at 0.1C (Figure S3a). For LNCMO-1090, the reversible capacities of fresh and stored cathode drop to 144 mAh g^{-1} and 125 mAh g^{-1} when increasing the rate to 2C (Figure S2c and S2d), which is 70% and 58% of the initial capacity at 0.1C (Figure S3b). Although the rate capability of cathode materials deteriorates after storage, LNCMO-1090 exhibits a slower capacity decay compared to NCM-811, which is correlated with the relatively stable surface structure of LNCMO-1090.

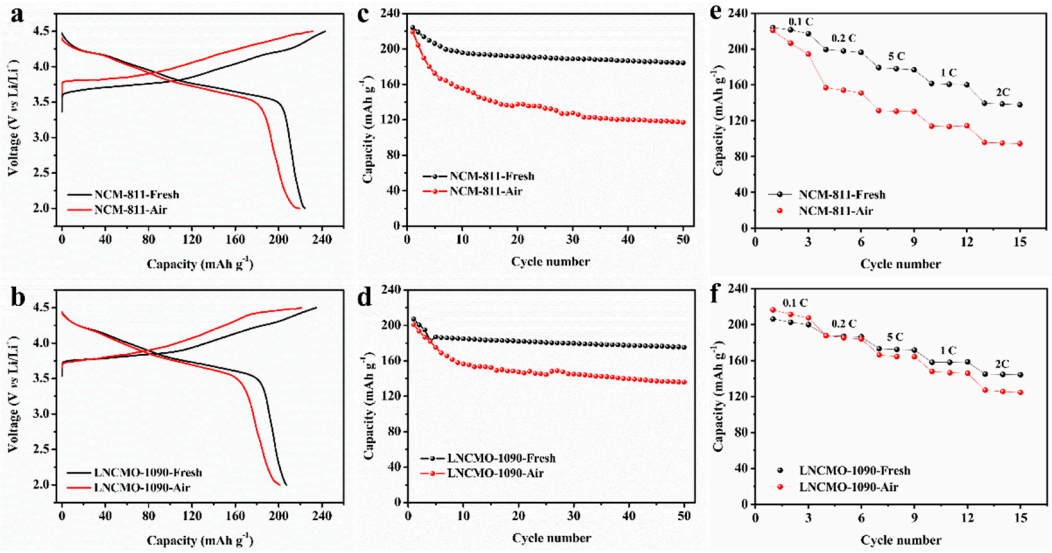

Figure 6. Comparison of electrochemical performance of cathode materials before and after storage: (**a**, **b**) first charge/discharge profiles at 0.1 C; (**c**, **d**) cycling performance at 0.1 C; (**e**, **f**) rate capability.

3.3. Thermal Stability of Ni-rich Layered Cathodes

The safety characteristic of LIBs is a very important indicator for their practical application, which depends strongly on the thermal stability of the electrode material [39–41]. Driven by the elevated temperature, the delithiated layered cathodes suffer the serious structural transformation from layered phase to spinel and rock-salt phase, accompanied by oxygen release which accelerates the combustion of electrolyte to lead the serious thermal runaway or even explosion [42–46]. Firstly, the heat release of the Ni-rich cathode with varied delithiation states was investigated using a differential scanning calorimeter (DSC). The delithiation states of NCM-811 cathodes are controlled by changing charge voltage. As shown in Figure 7a, the heat release of NCM-811-4.3V, responding to the structure transformation and oxygen release [27,47], begins to occur when the temperature rises above 200 °C, and a weak peak appears at 220 °C. With further elevated temperatures, more severe structure degradation results in more oxygen release from the oxide lattice, thereby accelerating the combustion of electrolyte to generate an exothermic peak at approximately 272 °C. The total heat release of NCM-811-4.3V during the exothermic reaction is counted as 1270 J g^{-1}. In higher delithiation states, the initiation of heat release of NCM-811-4.5V and NCM-811-4.8V occurs at a lower temperature below 200 °C, and the exothermic peak shifts to a lower temperature of 205 °C. For the whole exothermic reaction during elevating temperature, the heat release of NCM-811-4.5V and NCM-811-4.8V is evaluated as 1312 J g^{-1} and 1336 J g^{-1}, respectively. The heat release of the delithiated Ni-rich cathodes increases with the increased charge states. The higher delithiation induces more Ni^{4+} ions in the cathodes, and more substantial oxygen release, which is well confirmed by the more obvious exothermic peak of NCM-811-4.5V and NCM-811-4.8V at 203 °C. Furthermore, the influence of introducing Li_2MnO_3 on the thermal stability of the Ni-rich layered cathode was evaluated by DSC (Figure 7b). When charged to 4.5 V, NCM-811-4.5V shows a clear exothermic peak for phase transition at about 200 °C, while this peak becomes very weak and flat in LNCMO-1090-4.5V. This result

Preprints (www.preprints.org) | NOT PEER-REVIEWED | Posted: 5 January 2024 doi:10.20944/preprints202401.0450.v1

indicates that introducing Li_2MnO_3 reduces the oxygen release and impedes the phase transition behavior of the Ni-rich cathode. Meanwhile, the heat release of the delithiated cathodes decreases from 1312 J g^{-1} of NCM-811 to 891 J g^{-1} of LNCMO-1090. It can be found that LNCMO-1090 exhibits more excellent thermal stability than NCM-811. Introducing layered Li_2MnO_3 into a Ni-rich layered cathode can increase the stable Mn component and reduce the active Ni component in the formed solid-solution cathode, thereby inhibiting the oxygen release and phase transition to reduce the heat release.

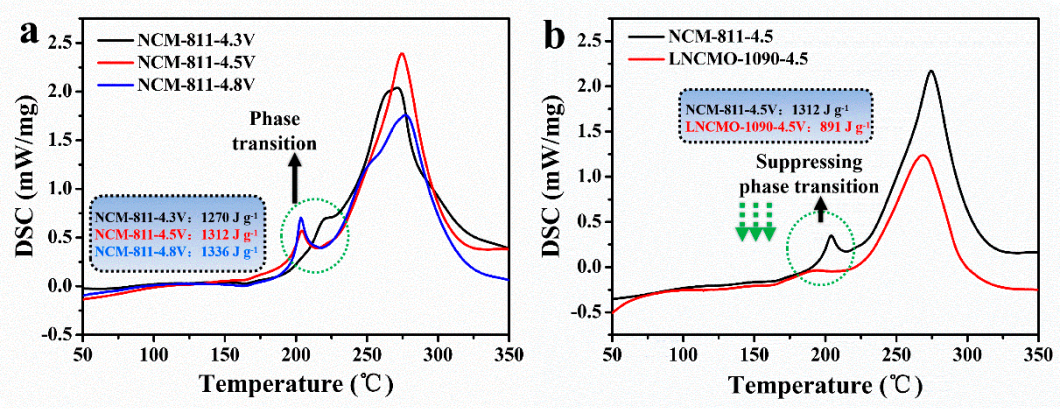

Figure 7. (**a**) The DSC curves of NCM-811 cathode with different charge states; (**b**) the DSC curves of NCM-811 and LNCMO-1090 cathodes with charge state of 4.5 V vs Li/Li^+.

4. Conclusions

In conclusion, the effect of introducing Li_2MnO_3 on the storage performance and thermal stability of Ni-rich cathode were investigated. The physical characterization results indicate that a dense and thick Li_2CO_3 layer produces on the surface of Ni-rich layered cathode during storage in air due to its high surface reactivities. This Li_2CO_3 impurity layer increases the electrode impedance and accelerates the cathode/electrolyte side reaction, resulting in the severe structural degradation and electrolyte decomposition. Consequently, Ni-rich cathode after long-term storage exhibits a remarkable deterioration in the reversible capacity, cycling stability and rate capability. Introducing Li_2MnO_3 into Ni-rich cathode can increase Mn component and reduce Ni component on cathode surface, thereby reducing its surface reactivity and sensitivity to air. Therefore, the formed solid-solution cathode (LNCMO-1090) exhibits a significant inhibition effect on deterioration of electrochemical performance after storage in air, which could be attributed to the thinner Li_2CO_3 impurity layer forming on LNCMO-1090 surface. Furthermore, DSC test results show that the heat release of Ni-rich cathode strongly depends on the delithiation states (charge voltage), which is closely linked with oxygen release. Introduction of Li_2MnO_3 has a remarkable suppression effect on oxygen release from Ni-rich cathode. Therefore, LNCMO-1090 displays more excellent thermal stability compared with NCM-811. This work opens up a new method to enhance the structural and thermal stability of Ni-rich layered cathode and offers a new idea for the rational design of advanced cathode materials.

Supplementary Materials: The following supporting information can be downloaded at the website of this paper posted on Preprints.org, Table S1: fitting values of the electrochemical impedance (EIS) curves of the cathodes charged to 4.3 V before and after storage obtained from equivalent circuit in the inset of Figure 5; Table S2: fhe first discharge capacity and 50th discharge capacity before and after storage and the capacity retention after 50 cycles at 0.1 C of the cathode materials of NCM-811 and LNCMO-1090; Figure S1: the charge/discharge profiles at different cycles of (a, b) the NCM-811 and (c, d) LNCMO-1090 cathodes before and after storage at a rate of 0.1 C between 2.0 and 4.5 V vs Li/Li^+: (a, c) before storage, (b, d) after storage; Figure S2: the charge/discharge profiles at different rates of (a, b) the NCM-811 and (c, d) LNCMO-1090 cathodes before and after storage between 2.0 and 4.5 V vs Li/Li^+: (a, c) before storage, (b, d) after storage; Figure S3: the capacity retention at different rates of (a, b) the NCM-811 and (c, d) LNCMO-1090 cathodes before and after storage between 2.0 and 4.5 V vs Li/Li^+.

Author Contributions: Conceptualization, J.Y.; validation, H.W.; investigation, J.Y.; resources, J.Y.; data curation, P.Y.; writing—original draft preparation, P.Y.; writing—review and editing, J.Y. and H.W.; visualization, P.Y.; supervision, H.W.; formal analysis, P.Y.; software, P.Y.; All authors have read and agreed to the published version of the manuscript.

Funding: This research was funded by the Program of Science and Technology International Cooperation Project of Qinghai Province (2022-HZ-811), and the National Natural Science Foundation of China (22279076, 21805179).

Data Availability Statement: Data are contained within the article and **Supplementary Materials**.

Conflicts of Interest: The authors declare no conflicts of interest.

References

1. Shi, C.-G.; Peng, X.; Dai, P.; Xiao, P.; Zheng, W.-C.; Li, H.-Y.; Li, H.; Indris, S.; Mangold, S.; Hong, Y.-H.; Luo, C.-X.; Shen, C.-H.; Wei, Y.-M.; Huang, L.; Sun, S.-G. Investigation and Suppression of Oxygen Release by $LiNi_{0.8}Co_{0.1}Mn_{0.1}O_2$ Cathode under Overcharge Conditions. *Adv. Energy Mater.* **2022**, *12*, 2200569.
2. Liu, Y. J.; Zeng, T. Y.; Li, G. T.; Wan, T.; Li, M. Y.; Zhang, X. Y.; Li, M. Q.; Su, M. R.; Dou, A. C.; Zeng, W. S.; Zhou, Y.; Guo, R. Q.; Chu, D. W. The surface double-coupling on single-crystal $LiNi_{0.8}Co_{0.1}Mn_{0.1}O_2$ for inhibiting the formation of intragranular cracks and oxygen vacancies. *Energy Storage Mater.* **2022**, *52*, 534-546.
3. Freiberg, A. T. S.; Sicklinger, J.; Solchenbach, S.; Gasteiger, H. A. Li_2CO_3 decomposition in Li-ion batteries induced by the electrochemical oxidation of the electrolyte and of electrolyte impurities. *Electrochim. Acta* **2020**, *346*, 136271.
4. Kang, H. S.; Santhoshkumar, P.; Park, J. W.; Sim, G. S.; Nanthagopal, M.; Lee, C. W. Glass ceramic coating on $LiNi_{0.8}Co_{0.1}Mn_{0.1}O_2$ cathode for Li-ion batteries. *Korean J. Chem. Eng.* **2020**, *37*, 1331-1339.
5. Wood, M.; Li, J. L.; Ruther, R. E.; Du, Z. J.; Self, E. C.; Meyer, H. M.; Daniel, C.; Belharouak, I.; Wood, D. L. Chemical stability and long-term cell performance of low-cobalt, Ni-rich cathodes prepared by aqueous processing for high-energy Li-ion batteries. *Energy Storage Mater.* **2020**, *24*, 188-197.
6. Zheng, W.-C.; Shi, C.-G.; Dai, P.; Huang, Z.; Lin, J.-X.; Chen, H.; Sun, M.-L.; Shen, C.-H.; Luo, C.-X.; Wang, Q.; Feng, X.; Wei, Y.-M.; Huang, L.; Sun, S.-G. A functional electrolyte additive enabling robust interphases in high-voltage $Li||LiNi_{0.8}Co_{0.1}Mn_{0.1}O_2$ batteries at elevated temperatures. *J. Mater. Chem. A* **2022**, *10*, 21912-21922.
7. Liu, J. X.; Wang, J. Q.; Ni, Y. X.; Zhang, K.; Cheng, F. Y.; Chen, J. Recent breakthroughs and perspectives of high-energy layered oxide cathode materials for lithium ion batteries. *Mater. Today* **2021**, *43*, 132-165.
8. Li, Y.; Liu, X.; Wang, L.; Feng, X. N.; Ren, D. S.; Wu, Y.; Xu, G. L.; Lu, L. G.; Hou, J. X.; Zhang, W. F.; Wang, Y. L.; Xu, W. Q.; Ren, Y.; Wang, Z. F.; Huang, J. Y.; Meng, X. F.; Han, X. B.; Wang, H. W.; He, X. M.; Chen, Z. H.; Amine, K.; Ouyang, M. Thermal runaway mechanism of lithium-ion battery with $LiNi_{0.8}Co_{0.1}Mn_{0.1}O_2$ cathode materials. *Nano Energy* **2021**, *85*, 105878.
9. Xue, W. J.; Huang, M. J.; Li, Y. T.; Zhu, Y. G.; Gao, R.; Xiao, X. H.; Zhang, W. X.; Li, S. P.; Xu, G. Y.; Yu, Y.; Li, P.; Lopez, J.; Yu, D. W.; Dong, Y. H.; Fan, W. W.; Shi, Z.; Xiong, R.; Sun, C.-J.; Hwang, I.; Lee, W.-K.; Shao-Horn, Y.; Johnson, J. A.; Li, J. Ultra-high-voltage Ni-rich layered cathodes in practical Li metal batteries enabled by a sulfonamide-based electrolyte. *Nat. Energy* **2021**, *6*, 495-505.
10. Wang, C. H.; Shao, L.; Guo, X.; Xi, X. M.; Yang, L. S.; Huang, C. H.; Zhou, C. X.; Zhao, H. H.; Yin, D. L.; Wang, Z. C. Air-Induced Degradation and Electrochemical Regeneration for the Performance of Layered Ni-Rich Cathodes. *ACS Appl. Mater. Inter.* **2019**, *11*, 44036-44045.
11. Sun, P. P.; Du, F. H.; Zhou, Q.; Hu, D.; Xu, T.; Mei, C. X.; Hao, Q.; Fan, Z. X.; Zheng, J. W. Efficient preservation of surface state of $LiNi_{0.82}Co_{0.15}Al_{0.03}O_2$ through assembly of hydride terminated polydimethylsiloxane. *J. Power Sources* **2021**, *495*, 229761.
12. Zeng, L. C.; Shi, K. X.; Qiu, B.; Liang, H. Y.; Li, J. H.; Zhao, W.; Li, S. L.; Zhang, W. G.; Liu, Z. P.; Liu, Q. B. Hydrophobic surface coating against chemical environmental instability for Ni-rich layered oxide cathode materials. *Chem. Eng. J.* **2022**, *437*, 135276.
13. Xie, Q.; Li, W. D.; Manthiram, A., A Mg-Doped High-Nickel Layered Oxide Cathode Enabling Safer, High-Energy-Density Li-Ion Batteries. *Chem. Mater.* **2019**, *31*, 938-946.
14. Han, G.-M.; Kim, Y.-S.; Ryu, H.-H.; Sun, Y.-K.; Yoon, C. S. Structural Stability of Single-Crystalline Ni-Rich Layered Cathode upon Delithiation. *ACS Energy Lett.* **2022**, *7*, 2919-2926.
15. Liu, B.; Jia, Y.; Yuan, C.; Wang, L.; Gao, X.; Yin, S.; Xu, J. Safety issues and mechanisms of lithium-ion battery cell upon mechanical abusive loading: A review. *Energy Storage Mater.* **2020**, *24*, 85-112.
16. Li, L. J.; Fu, L. Z.; Li, M.; Wang, C.; Zhao, Z. X.; Xie, S. C.; Lin, H. C.; Wu, X. W.; Liu, H. D.; Zhang, L.; Zhang, Q. B.; Tan, L., B-doped and La_4NiLiO_8-coated Ni-rich cathode with enhanced structural and interfacial stability for lithium-ion batteries. *J. Energy Chem.* **2022,** *71*, 588-594.

17. Fan, X. M.; Ou, X.; Zhao, W. G.; Liu, Y.; Zhang, B.; Zhang, J. F.; Zou, L. F.; Seidl, L.; Li, Y. Z.; Hu, G. R.; Battaglia, C.; Yang, Y., In situ inorganic conductive network formation in high-voltage single-crystal Ni-rich cathodes. *Nat. Commun.* **2021,** *12*, 5320.
18. Yin, S. Y.; Deng, W. T.; Chen, J.; Gao, X.; Zou, G. Q.; Hou, H. S.; Ji, X. B., Fundamental and solutions of microcrack in Ni-rich layered oxide cathode materials of lithium-ion batteries. *Nano Energy* **2021,** *83*, 105854.
19. Yang, J.; Xia, Y., Enhancement on the Cycling Stability of the Layered Ni-Rich Oxide Cathode by In-Situ Fabricating Nano-Thickness Cation-Mixing Layers. *J. Electrochem. Soc.* **2016**, *163*, A2665-A2672.
20. Noh, H.-J.; Youn, S.; Yoon, C. S.; Sun, Y.-K., Comparison of the structural and electrochemical properties of layered $Li[Ni_xCo_yMn_z]O_2$ (x = 1/3, 0.5, 0.6, 0.7, 0.8 and 0.85) cathode material for lithium-ion batteries. *J. Power Sources* **2013,** *233*, 121-130.
21. Yang, J.; Hou, M.; Haller, S.; Wang, Y.; Wang, C.; Xia, Y. Improving the Cycling Performance of the Layered Ni-Rich Oxide Cathode by Introducing Low-Content Li_2MnO_3. *Electrochim. Acta* **2016**, *189*, 101-110.
22. Yang, J.; Xia, Y. Suppressing the Phase Transition of the Layered Ni-Rich Oxide Cathode during High-Voltage Cycling by Introducing Low-Content Li_2MnO_3. *ACS Appl. Mater. Inter.* **2016**, *8*, 1297-1308.
23. Jeong, M.; Kim, H.; Lee, W.; Ahn, S.-J.; Lee, E.; Yoon, W.-S. Stabilizing effects of Al-doping on Ni-rich $LiNi_{0.80}Co_{0.15}Mn_{0.05}O_2$ cathode for Li rechargeable batteries. *J. Power Sources* **2020**, *474*, 228592.
24. Becker, D.; Boerner, M.; Noelle, R.; Diehl, M.; Klein, S.; Rodehorst, U.; Schmuch, R.; Winter, M.; Placke, T. Surface Modification of Ni-Rich $LiNi_{0.8}Co_{0.1}Mn_{0.1}O_2$ Cathode Material by Tungsten Oxide Coating for Improved Electrochemical Performance in Lithium-Ion Batteries. *ACS Appl. Mater. Inter.* **2019**, *11*, 18404-18414.
25. Andersen, H. L.; Cheung, E. A.; Avdeev, M.; Maynard-Casely, H. E.; Abraham, D. P.; Sharma, N., Consequences of long-term water exposure for bulk crystal structure and surface composition/chemistry of nickel-rich layered oxide materials for Li-ion batteries. *J. Power Sources* **2020,** *470*, 228370.
26. Xu, C. L.; Xiang, W.; Wu, Z. G.; Qiu, L.; Ming, Y.; Yang, W.; Yue, L. C.; Zhang, J.; Zhong, B. H.; Guo, X. D.; Wang, G. K.; Liu, Y. X., Dual-site lattice modification regulated cationic ordering for Ni-rich cathode towards boosted structural integrity and cycle stability. *Chem. Eng. J.* **2021,** *403*, 126314.
27. Zhou, K.; Xie, Q.; Li, B. H.; Manthiram, A., An in-depth understanding of the effect of aluminum doping in high-nickel cathodes for lithium-ion batteries. *Energy Storage Mater.* **2021,** *34*, 229-240.
28. Tang, M.; Yang, J.; Chen, N.; Zhu, S.; Wang, X.; Wang, T.; Zhang, C.; Xia, Y. Overall structural modification of a layered Ni-rich cathode for enhanced cycling stability and rate capability at high voltage. *J. Mater. Chem. A* **2019**, *7*, 6080-6089.
29. Zhang, F.; Lou, S. F.; Li, S.; Yu, Z. J.; Liu, Q. S.; Dai, A.; Cao, C. T.; Toney, M. F.; Ge, M. Y.; Xiao, X. H.; Lee, W. K.; Yao, Y. D.; Deng, J. J.; Liu, T. C.; Tang, Y. P.; Yin, G. P.; Lu, J.; Su, D.; Wang, J. J., Surface regulation enables high stability of single-crystal lithium-ion cathodes at high voltage. *Nat. Commun.* **2020,** *11*, 3050.
30. Feng, Y.; Xu, H.; Wang, B.; Tuo, K.; Wang, P.; Wang, S.; Liang, W.; Lu, H.; Li, S. Structural evolution of nickel-rich layered cathode material $LiNi_{0.8}Co_{0.1}Mn_{0.1}O_2$ at different current rates. *Ionics* **2021**, *27*, 517-526.
31. Yin, E.; Grimaud, A.; Rousse, G.; Abakumov, A. M.; Senyshyn, A.; Zhang, L.; Trabesinger, S.; Iadecola, A.; Foix, D.; Giaume, D.; Tarascon, J.-M. Structural evolution at the oxidative and reductive limits in the first electrochemical cycle of $Li_{1.2}Ni_{0.13}Mn_{0.54}Co_{0.13}O_2$. *Nat. Commun.* **2020**, *11*, 1252.
32. Xiong, C.; Fu, H. K.; Wu, L. J.; Yuan, G. Q. Enhanced Electrochemical Performance of $LiNi_{0.8}Co_{0.1}Mn_{0.1}O_2$ Cathode Material for lithium ion batteries by WO_3 surface coating. *Int. J. Electrochem. Sc.* **2020**, *15*, 8990-9002.
33. Liu, X. S.; Zheng, B. Z.; Zhao, J.; Zhao, W. M.; Liang, Z. T.; Su, Y.; Xie, C. P.; Zhou, K.; Xiang, Y. X.; Zhu, J. P.; Wang, H. C.; Zhong, G. M.; Gong, Z. L.; Huang, J. Y.; Yang, Y., Electrochemo-Mechanical Effects on Structural Integrity of Ni-Rich Cathodes with Different Microstructures in All Solid-State Batteries. *Adv. Energy Mater.* **2021,** *11*, 2003583.
34. Li, X. L.; Jin, L. B.; Song, D. W.; Zhang, H. Z.; Shi, X. X.; Wang, Z. Y.; Zhang, L. Q.; Zhu, L. Y., $LiNbO_3$-coated $LiNi_{0.8}Co_{0.1}Mn_{0.1}O_2$ cathode with high discharge capacity and rate performance for all-solid-state lithium battery. *J. Energy Chem.* **2020,** *40*, 39-45.
35. Lee, S. H.; Park, G. J.; Sim, S. J.; Jin, B. S.; Kim, H. S. Improved electrochemical performances of $LiNi_{0.8}Co_{0.1}Mn_{0.1}O_2$ cathode via SiO_2 coating. *J. Alloy. Compd.* **2019**, *791*, 193-199.
36. Li, Y. J.; Deng, S. Y.; Chen, Y. X.; Gao, J.; Zhu, J.; Xue, L. L.; Lei, T. X.; Cao, G. L.; Guo, J.; Wang, S. L. Dual functions of residue Li-reactive coating with $C_4H_6CoO_4$ on high-performance $LiNiO_2$ cathode material. *Electrochim. Acta* **2019**, *300*, 26-35.
37. Zhang, Y. R.; Katayama, Y.; Tatara, R.; Giordano, L.; Yu, Y.; Fraggedakis, D.; Sun, J. G. W.; Maglia, F.; Jung, R.; Bazant, M. Z.; Shao-Horn, Y., Revealing electrolyte oxidation via carbonate dehydrogenation on Ni-based oxides in Li-ion batteries by in situ Fourier transform infrared spectroscopy. *Energ. Environ. Sci.* **2020,** *13*, 183-199.
38. Cheng, W. D.; Hao, S.; Ji, Y. Y.; Li, L.; Liu, L.; Xiao, Y.; Wu, Y. X.; Huo, J. S.; Tang, F.; Liu, X. Q., Optimizing surface residual alkali and enhancing electrochemical performance of $LiNi_{0.8}Co_{0.15}Al_{0.05}O_2$ cathode by LiH_2PO_4. *Nanotechnology* **2022,** *33*, 045404.

39. Zuo, T.-T.; Ruess, R.; Pan, R.; Walther, F.; Rohnke, M.; Hori, S.; Kanno, R.; Schroeder, D.; Janek, J. A mechanistic investigation of the $Li_{10}GeP_2S_{12}$|$LiNi_{1-x-y}Co_xMn_yO_2$ interface stability in all-solid-state lithium batteries. *Nat. Commun.* **2021**, *12*, 6669.
40. Liu, S. F.; Ji, X.; Yue, J.; Hou, S.; Wang, P. F.; Cui, C. Y.; Chen, J.; Shao, B. W.; Li, J. R.; Han, F. D.; Tu, J. P.; Wang, C. S., High Interfacial-Energy Interphase Promoting Safe Lithium Metal Batteries. *J. Am. Chem. Soc.* **2020,** *142*, 2438-2447.
41. Yang, J.; Liang X. H., Ryu H. H.; Yoon, C. S.; Sun Y. K., Ni-Rich Layered Cathodes for Lithium-Ion Batteries: From Challenges to the Future. *Energy Storage Mater.* **2023**, *63*, 102969.
42. Jung, S. H.; Kim, U. H.; Kim, J. H.; Jun, S. G.; Yoon, C. S.; Jung, Y. S.; Sun, Y. K. Ni-Rich Layered Cathode Materials with Electrochemo-Mechanically Compliant Microstructures for All-Solid-State Li Batteries. *Adv. Energy Mater.* **2020**, *10*, 1903360.
43. Xu, G. L.; Liu, X.; Daali, A.; Amine, R.; Chen, Z. H.; Amine, K. Challenges and Strategies to Advance High-Energy Nickel-Rich Layered Lithium Transition Metal Oxide Cathodes for Harsh Operation. *Adv. Funct. Mater.* **2020**, *30*, 2004748.
44. Wang, Q. D.; Yao, Z. P.; Zhao, C. L.; Verhallen, T.; Tabor, D. P.; Liu, M.; Ooms, F.; Kang, F. Y.; Aspuru-Guzik, A.; Hu, Y. S.; Wagemaker, M.; Li, B. H., Interface chemistry of an amide electrolyte for highly reversible lithium metal batteries. *Nat. Commun.* **2020,** *11*, 4188.
45. He, W.; Guo, W. B.; Wu, H. L.; Lin, L.; Liu, Q.; Han, X.; Xie, Q. S.; Liu, P. F.; Zheng, H. F.; Wang, L. S.; Yu, X. Q.; Peng, D. L., Challenges and Recent Advances in High Capacity Li-Rich Cathode Materials for High Energy Density Lithium-Ion Batteries. *Adv. Mater.* **2021,** *33*, 2005937.
46. Ren, D. S.; Feng, X. N.; Liu, L. S.; Hsu, H. J.; Lu, L. G.; Wang, L.; He, X. M.; Ouyang, M. G. Investigating the relationship between internal short circuit and thermal runaway of lithium-ion batteries under thermal abuse condition. *Energy Storage Mater.* **2021,** *34*, 563-573.
47. Csernica, P. M.; Kalirai, S. S.; Gent, W. E.; Lim, K.; Yu, Y. S.; Liu, Y. Z.; Ahn, S. J.; Kaeli, E.; Xu, X.; Stone, K. H.; Marshall, A. F.; Sinclair, R.; Shapiro, D. A.; Toney, M. F.; Chueh, W. C., Persistent and partially mobile oxygen vacancies in Li-rich layered oxides. *Nat. Energy* **2021,** *6*, 642-652.